Available online at www.sciencedirect.com
ScienceDirect
Trans. Nonferrous Met. Soc. China 34(2024) 3905−3918
Transactions of Nonferrous Metals Society of China
www.tnmsc.cn

Microstructure evolution and hot workability of in-situ synthesized Ti_2AlC/TiAl composite

Yu-peng WANG[1], Teng-fei MA[1,2], Lei LI[1], Long-long DONG[1], Wang-tu HUO[1], Yu-sheng ZHANG[1], Lian ZHOU[1]

1. Northwest Institute for Non-ferrous Metal Research, Xi'an 710016, China;
2. Key Laboratory of Air-driven Equipment Technology of Zhejiang Province, Quzhou University, Quzhou 324000, China

Received 5 May 2023; accepted 8 November 2023

Abstract: The in-situ micro-nano Ti_2AlC particles reinforced TiAl (Ti_2AlC/TiAl) composite was fabricated using spark plasma sintering. The hot workability of Ti_2AlC/TiAl composite was studied, and the effect of micro-nano particles on flow stress and dynamic recrystallization of composite was discussed. The results showed that the micro-nano Ti_2AlC particles included strengthening and softening effects during hot deformation, resulting in the fact that the Ti_2AlC/TiAl composite exhibited a higher flow stress and more sufficient dynamic recrystallization. The strengthening effect was mainly attributed to the Ti_2AlC particles induced refinement strengthening and hindered dislocation motion at the initial stage. Moreover, the precipitation of nano-$TiCr_2$ particles induced by stress concentration during hot deformation also contributed to higher flow stress via impeding dislocation motion. Meanwhile, the refined microstructure and dislocation pile-up caused by micro-nano particles during deformation provided more nucleation sites for dynamic recrystallization, which significantly promoted the dynamic recrystallization of the second stage. The present results reveal that the Ti_2AlC/TiAl composite exhibited excellent hot workability, which is important to promote the application of TiAl alloys.

Key words: Ti_2AlC/TiAl composite; spark plasma sintering; hot deformation; microstructure evolution; dynamic recrystallization

1 Introduction

TiAl alloys are considered as outstanding lightweight structural materials, which are suitable for the aerospace field [1,2]. Typically, TiAl-based turbine blades have been successfully applied, for example, the low-pressure turbine blades of PW1100G aero-engine were fabricated using Ti−43Al−4Nb−1Mo−0.1B alloys and successfully applied on Airbus A320neo aircraft. Similarly, Ti−48Al−2Cr−2Nb alloys have successfully employed in the sixth and seventh turbine blades of GEnx^{TM}-2B aero-engines, serving the Boeing 747-8 aircraft [2]. However, the broader applications of TiAl alloys have been limited by their poor room temperature ductility and high-temperature mechanical properties [3,4].

Recently, the TiAl composites have been successfully fabricated using spark plasma sintering (SPS), vacuum arc re-melting (VAR), and induction skull melting (ISM), resulting in the enhancement of the mechanical properties of TiAl alloys significantly [5−7]. Specifically, DING et al [6] successfully synthesized (TiB/Ti)−TiAl composites with a laminated structure via SPS, and the bending fracture strength and fracture toughness were improved remarkably at room temperature. FANG

Corresponding author: Teng-fei MA, Tel: +86-571-8026716, E-mail: matengfeihit@163.com
DOI: 10.1016/S1003-6326(24)66647-1

et al [7] reported a TiAl composite with multi-scale reinforcing phase, which showed a notable tensile strength of 541 MPa with a fracture strain of 8.9% at 850 °C. In particular, Ti_2AlC with a layered ternary is an exemplary reinforcement phase that combined the characteristics of metals and ceramics, demonstrating exceptional fracture resistance, electrical conductivity, and hot conductivity [8,9]. And in-situ synthesis of Ti_2AlC-reinforced TiAl composites has been successfully achieved by adding multilayer graphene, nano-C powder, and other carbon sources to TiAl alloys. WU et al [10,11] found that Ti_2AlC particles can be directly synthesized by solid-phase sintering at the interfaces between the TiAl matrix and multilayer graphene, devoid of the formation of TiC mesophase. This phenomenon was different from liquid-phase sintering. Furthermore, GUO et al [12] reported that micro-nano Ti_2AlC particles reinforced high-Nb TiAl composites were fabricated by hot-pressing sintering, and the Ti_2AlC particles were mainly distributed at the α_2/γ phase boundary, thereby significantly improved the high temperature tensile properties. This enhancement was primarily attributed to the combined mechanisms of refinement strengthening and precipitation strengthening. Notably, the micro-nano Ti_2AlC particles reinforced TiAl composites were also obtained by SPS in our previous work, which demonstrated excellent high temperature mechanical properties and oxidation resistance [13−15]. However, the hot deformation mechanisms and microstructure evolution of TiAl composites are seldom reported. While, this is necessary for their application.

Actually, the hot deformation behavior of TiAl alloys has been studied extensively, and the hot processing map was successfully established [16,17]. These results revealed that the strengthening and softening were strongly work hardening and dynamic recrystallization (DRX) softening dependent. Interestingly, the effect of particle reinforcement on the hot deformation behavior could not be neglected, because the interaction between the matrix and reinforcing phase leads to work hardening and dislocation pile-up, promoting DRX nucleation. Usually, the DRX nucleates preferentially at the grain boundaries and interfaces of reinforcing phase and matrix due to the high stress concentration. Then, DRX grains grow via interfacial diffusion and grain boundaries migration. For example, WANG et al [18] reported that the microstructural evolution of TiB_w/Ti60 composite was significantly affected by TiB_w. It was shown that the TiB_w provided high density dislocation and nucleation sites for DRX, and DRX of β grains occurred prior near TiB_w region.

In the present work, we mainly focused on the microstructure evolution and hot workability of micro-nano Ti_2AlC/TiAl composite with fully lamellar microstructure at different temperatures and strain rates, revealing the effect of micro-nano Ti_2AlC particles on hot deformation.

2 Experimental

In this experiment, the raw materials were spherical Ti−48Al−2Nb−2Cr (at.%) pre-alloyed powder (Sino-Euro Materials Technologies of Xi’an Co., Ltd., China) with a powder size range of 53−150 μm. Graphene oxide was purchased from XFNANO Co., Ltd., China. The pre-alloyed powder and graphene oxide were mixed by mechanical ball-milling for 360 min with 300 r/min, utilizing a zirconia ball-to-powder ratio of 3:1. Then, the mixed powder was sintered by SPS at a temperature of 1300 °C with a holding time of 5 min. And the applied pressure was 45 MPa. Finally, the sintered compacts with dimensions of d50 mm × 20 mm were obtained, and the compacts adding 0 and 0.5 wt.% graphene oxide were named as TiAl alloy and Ti_2AlC/TiAl composite, respectively.

Cylindrical specimens with 6 mm in diameter and 9 mm in height were cut by wire-electrode cutting from the sintered compacts. These specimens were subsequently subjected to hot deformation on a Gleeble−3800 hot simulation compression machine. The hot deformation temperature range was from 1100 to 1200 °C at a strain rate of 0.01−1 s^{-1}. And the samples were deformed to 60% (≈0.8 true strain). When deformation was completed, the samples were quenched in water immediately to reserve the deformed microstructure for subsequent analysis.

The phases were identified by X-ray diffractometer (XRD) with monochromatic Cu K_α radiation. The scanning angle changed from 20° to 90° with a constant step size of 5 (°)/min. For microstructure characterization, the metallographic samples were prepared and subsequently examined using optical microscopy (OM, Leica MPS30), scanning electron microscopy (SEM, Zeiss GeminiSEM500/HITACHI 8010) equipped with electron back scattered diffraction (EBSD). Besides, the structural characteristic of the sintered and deformed microstructure was further characterized by transmission electron microscopy (TEM, Talos F200C). For OM and SEM observation, the metallographic samples were prepared by using standard metallographic sample preparation methods. Subsequently, the samples were etched by a solution of 10 mL HF + 30 mL HNO_3 + 60 mL H_2O. For EBSD observation, longitudinal section of the deformed samples was electropolished at a temperature of −30 °C, utilizing a solution of 300 mL CH_4O + 150 mL $C_4H_{10}O$ + 50 mL $HClO_4$. A constant step size of 0.2 μm was applied, and the data was further processed utilizing Channel 5 software. For TEM observation, the specimens were cut from the sintered and deformed TiAl composites respectively, and then they were ground to <50 μm followed by ion-beam thinning.

3 Results

3.1 Initial microstructure

The microstructure of TiAl alloy and Ti_2AlC/TiAl composite exhibited a fully lamellar structure without obvious pores after sintering. This observation denoted that the samples with satisfied density were successfully obtained via SPS, as shown in Fig. 1. In addition, Figs. 1(a, b) showed that the average sizes of lamellar colonies in TiAl alloy and Ti_2AlC/TiAl composite were 362 and 140 μm, respectively. Evidently, the introduction of graphene oxide can refine the microstructure significantly. This was attributed to the precipitation of carbides, which effectively inhibited grain growth during the sintering. Figures 1(c, d) presented the corresponding SEM morphologies of sintered TiAl alloy and Ti_2AlC/TiAl composite, respectively. Obviously, the micro-nano particles precipitated at the interfaces between the α_2-Ti_3Al and γ-TiAl lamellae homogeneously in Ti_2AlC/TiAl composite, as illustrated in Fig. 1(d). A high carbon solid solubility in the α phase was achieved at high sintering temperature. Then, the secondary carbides precipitated from the interfaces of α_2-Ti_3Al and γ-Ti_3Al phase during cooling.

It is evident that the diffraction peaks of α_2-Ti_3Al and γ-TiAl phases are obvious, indicating that the TiAl alloy and Ti_2AlC/TiAl composite are mainly composed of γ and α_2 phases according to the XRD patterns displayed in Fig. 2. This observation can be attributed to the fact that the sintering temperature was located in the single α phase region, and the fully lamellar microstructure was obtained via the precipitation of γ lamellae from α_2 phase during cooling. This result was in

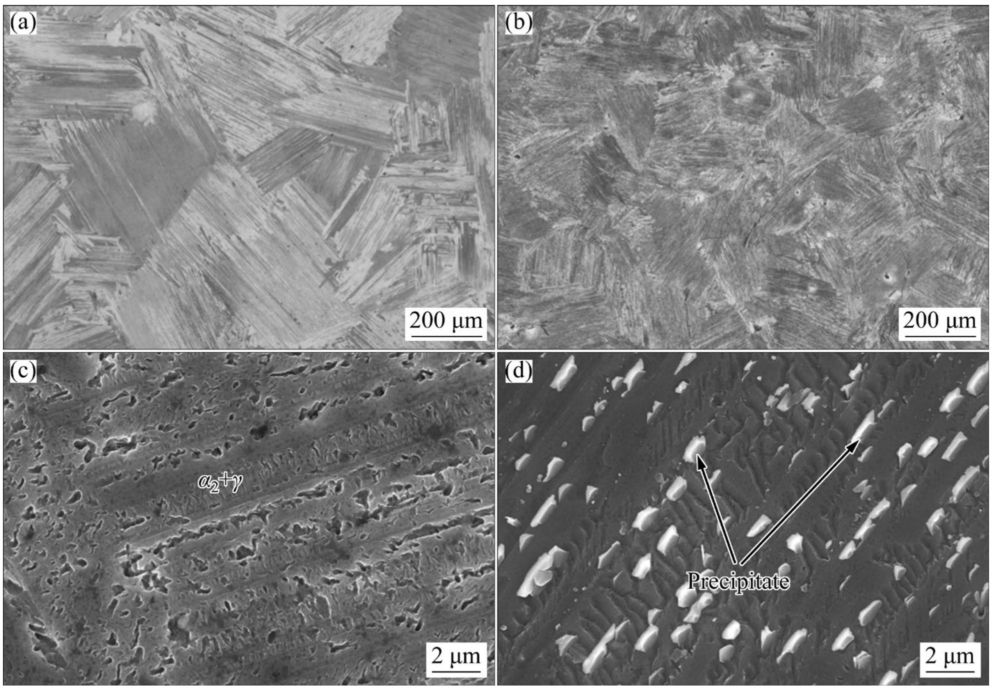

Fig. 1 OM (a, b) and SEM (c, d) images of TiAl alloy (a, c) and Ti_2AlC/TiAl composite (b, d)

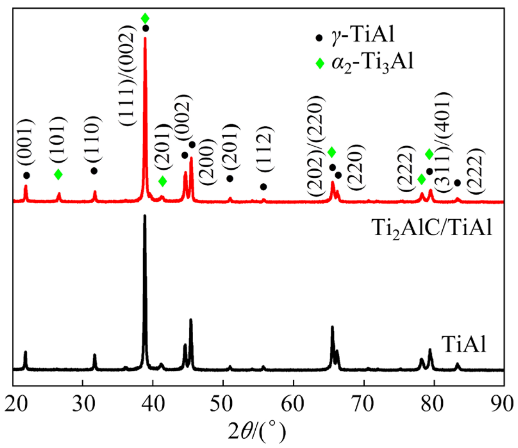

Fig. 2 XRD patterns of TiAl alloy and Ti_2AlC/TiAl composite

consensus with the findings in Fig. 1. In addition, the solubility of carbon atoms in TiAl alloys was limited, and carbides precipitated when beyond the solubility limit [19]. However, the diffraction peak associated with carbides was not detected in the Ti_2AlC/TiAl composite, due to their relatively low content, which will be further characterized later.

The microstructure of the Ti_2AlC/TiAl composite was further characterized using TEM, as shown in Fig. 3. High-angle annular dark field scanning transmission electron microscopy (HADDF-STEM) micrograph revealed the existence of three phases, which represented bright, gray and black, respectively, as exhibited in Fig. 3(a). The selected area electron diffractions (SAED) displayed in Figs. 3(b−e) demonstrated the crystalline structures of α_2-Ti_3Al (bright), γ-TiAl (gray) and the micro-nano particles (black). The micro-nano particles were identified to be Ti_2AlC phase according to the diffraction pattern analysis.

Figure 4(a) displayed a typical TEM image of the Ti_2AlC/TiAl composite under bright field (BF) pattern. Notably, a clean interface between Ti_2AlC particles and the TiAl matrix was observed,

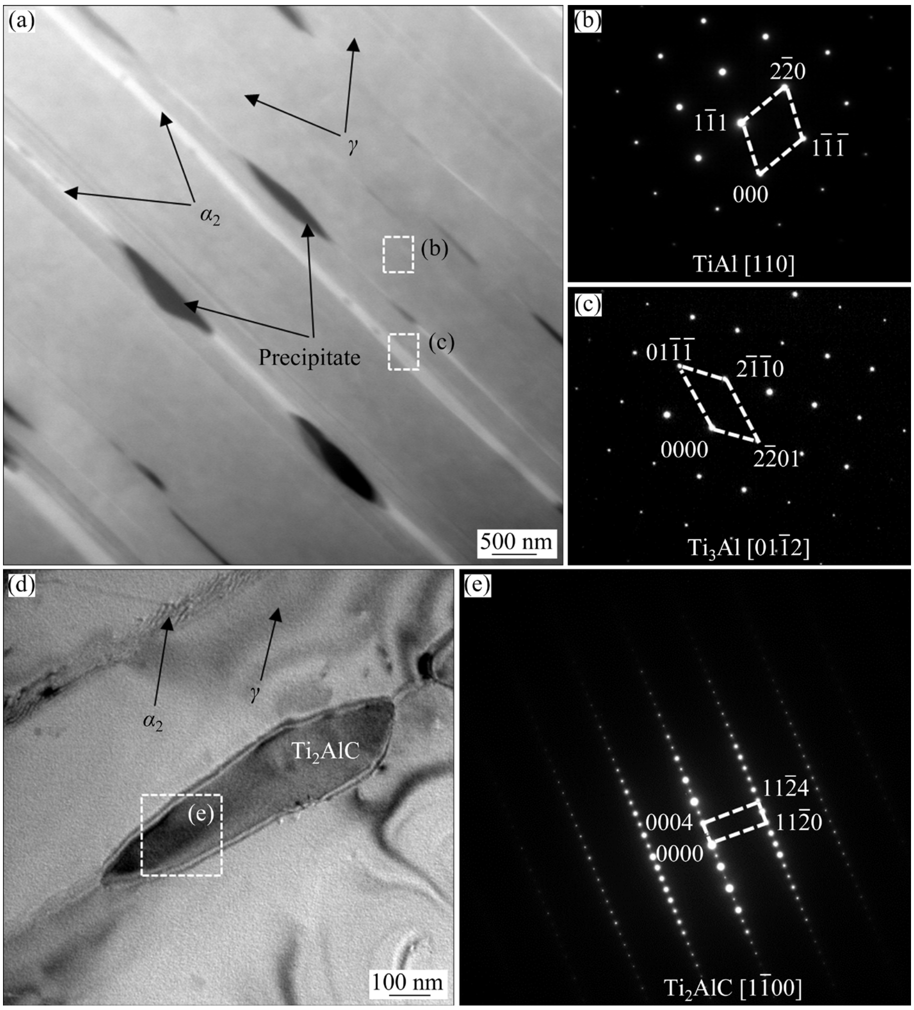

Fig. 3 TEM images of Ti_2AlC/TiAl composite: (a) HADDF-STEM micrograph; (b, c) SAED patterns of areas in (a); (d) Bright field of composite; (e) SAED pattern of area in (d)

denoting a good bond between Ti_2AlC particles and the TiAl matrix. The interface between Ti_2AlC and γ-TiAl phase was studied using HRTEM, and a semi-coherent interface was observed in Fig. 4(b). The orientation relationship between the Ti_2AlC and γ-TiAl interfaces was determined as $[2\bar{1}\bar{1}0]$ Ti_2AlC//[010]TiAl and (0001)Ti_2AlC//(001)TiAl according to the calibrated results presented in Fig. 4(b). In addition, the nano-twinning was observed around Ti_2AlC particles, as shown in Figs. 4(c, d). This is attributed to the formation of local stress concentration during sintering. These nano twin boundaries can hinder dislocation motion and provide additional nucleation sites as reported by LU et al [20]. Consequently, the hot deformation behavior of the Ti_2AlC/TiAl composite could be complex, which will be investigated further.

3.2 Flow behavior

Typical true stress−strain curves of TiAl alloy and Ti_2AlC/TiAl composite at different temperatures and strain rates were shown in Fig. 5.

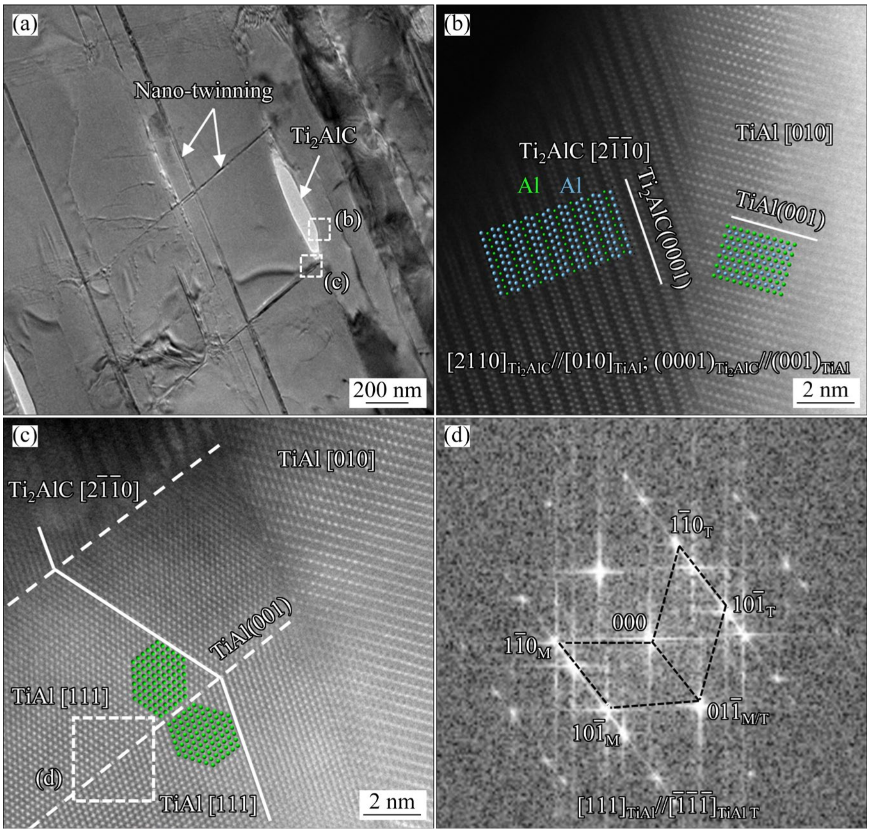

Fig. 4 TEM images of Ti_2AlC/TiAl composite: (a) BF micrograph; (b, c) HRTEM images of areas in (a); (d) FFT image of area in (c)

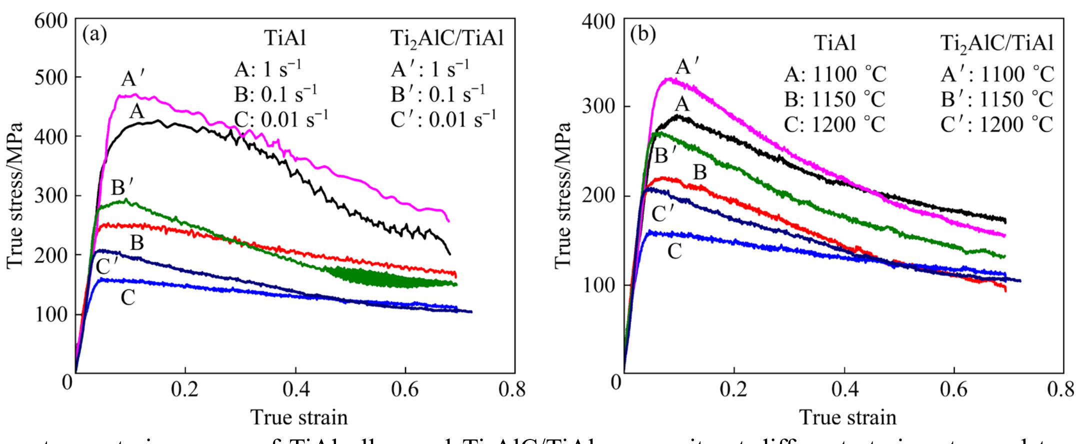

Fig. 5 True stress−strain curves of TiAl alloy and Ti_2AlC/TiAl composite at different strain rates and temperatures: (a) 1200 °C; (b) 0.01 s^{-1}

Apparently, all the curves exhibited typical characteristics of DRX softening: the flow stress increased sharply at the initial stage and reached a maximum, followed by a subsequent decrease due to the DRX. Moreover, it was observed that the peak stress decreased with increasing temperature and decreasing strain rate, revealing that the flow stress was sensitive to temperature and strain rate. For example, the peak stress of Ti_2AlC/TiAl composite decreased from 425.92 to 160.71 MPa as the strain rate decreased from 1 to 0.01 s^{-1} deformed at 1200 °C, as exhibited in Fig. 5(a). Similarly, the peak stress of Ti_2AlC/TiAl composite decreased from 331.35 to 204.28 MPa with an increase in deformation temperature from 1100 to 1200 °C under a constant strain rate of 0.01 s^{-1}, as shown in Fig. 5(b). The present results showed that the lower flow stress can be achieved by increasing the temperature or decreasing the strain rate.

Notably, it was worth noting that the peak stress was 204.28 MPa for Ti_2AlC/TiAl composite compared to that of 160.16 MPa for the TiAl alloy deformed at 1200 °C and 0.01 s^{-1}. This strengthening effect was primarily attributed to the refinement strengthening and precipitation strengthening. The intensive interaction between dislocation and Ti_2AlC particles in the Ti_2AlC/TiAl composite led to more pronounced work hardening at the initial deformation stage compared to TiAl alloy, which was beneficial to DRX. Consequently, an interesting result was observed that the flow stress was reduced more obviously in the Ti_2AlC/TiAl composite at the final stage. This phenomenon was related to DRX and will be discussed later.

3.3 Microstructural evolution

The deformed microstructures of TiAl alloy and Ti_2AlC/TiAl composite at different temperatures and a strain rate of 0.01 s^{-1} were shown in Fig. 6. Obviously, the lamellae were squashed perpendicularly to the compression direction, and the deformed microstructure exhibited more uniform with increasing deformation temperature. Specifically, the deformed microstructure of TiAl alloy consisted of deformed lamellar colonies and partially DRX grains at a lower temperature (1100 °C). It was revealed that the driving force for DRX was insufficient, as shown in Figs. 6(a, d). While, the residual lamellae decreased and DRX grains increased as the deformation temperature increased, exemplified by deformation at 1150 °C, 0.01 s^{-1} and 1200 °C, 0.01 s^{-1}. Higher temperature provided more driving force for deformation and DRX [21]. Furthermore, a band microstructure (complete DRX microstructure) was observed in Ti_2AlC/TiAl composite deformed at 1150 °C, 0.01 s^{-1} and 1200 °C, 0.01 s^{-1}, as shown in Figs. 6(e, f). It can be concluded that deformation was more uniform and DRX was more sufficient in Ti_2AlC/TiAl composite compared to TiAl alloy when subjected to the same deformation condition.

The deformed lamellar microstructure was further characterized using SEM to reveal the effect

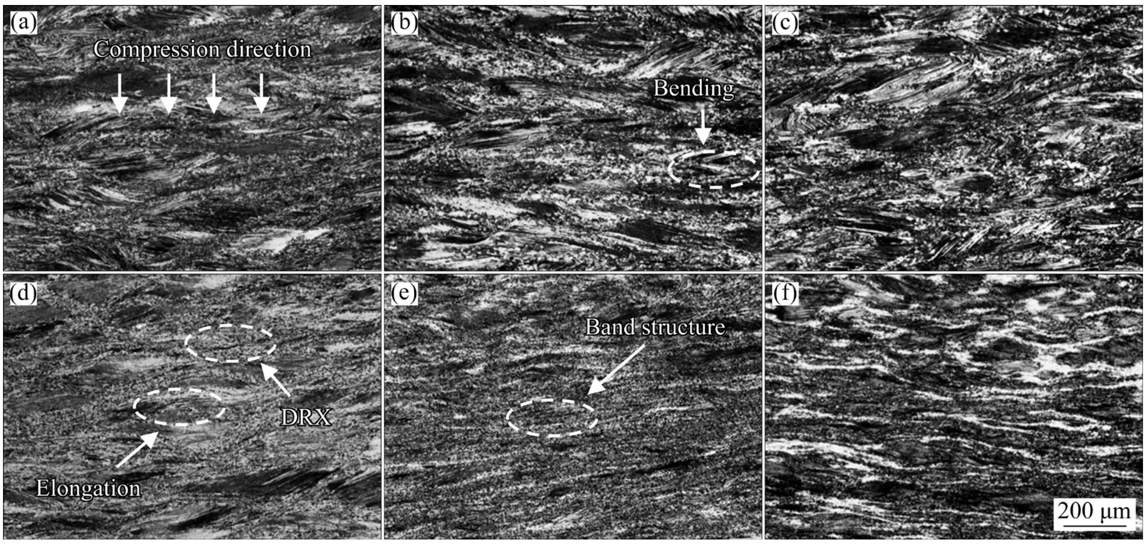

Fig. 6 Deformed microstructures of TiAl alloy and Ti_2AlC/TiAl composite: (a−c) TiAl alloy deformed at 0.01 s^{-1} and 1100, 1150 and 1200 °C, respectively; (d−f) Ti_2AlC/TiAl composite deformed at 0.01 s^{-1} and 1100, 1150 and 1200 °C, respectively

of micro-nano Ti_2AlC particles on the hot deformation behaviors. Clearly, the lamellae in TiAl alloy were bent and elongated during the hot deformation at 1200 °C and 0.01 s^{-1}, as shown in Fig. 7(a). For Ti_2AlC/TiAl composite, it can be found that the Ti_2AlC particles hindered lamellar deformation. In addition, it was observed that more DRX grains appeared around the Ti_2AlC particles (Figs. 7(b−d)), attributed to local stress concentration. These results indicated that the Ti_2AlC particles actively promoted the occurrence of DRX.

The typical deformed microstructure was further investigated using EBSD, and the corresponding results were presented in Figs. 8−10. The local misorientation map was shown in Fig. 8, and low and high misorientations displayed in blue and red, respectively. The partial residual lamellae

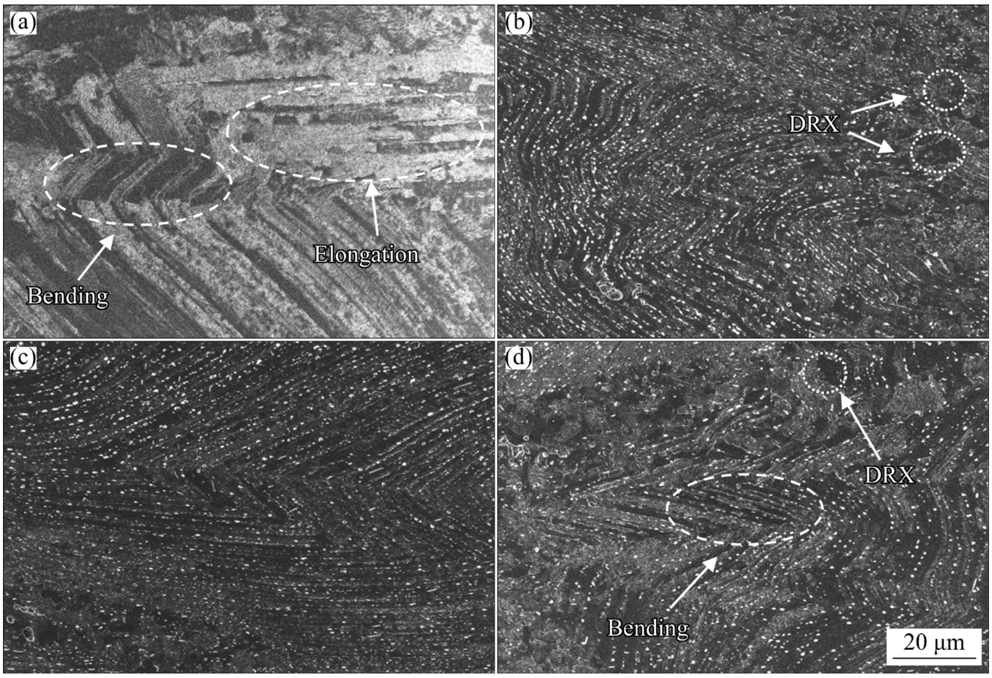

Fig. 7 Deformed microstructures of TiAl alloy and Ti_2AlC/TiAl composite deformed at 0.01 s^{-1} and different temperatures: (a) TiAl alloy at 1200 °C; (b−d) Ti_2AlC/TiAl composite at 1100, 1150, and 1200 °C, respectively

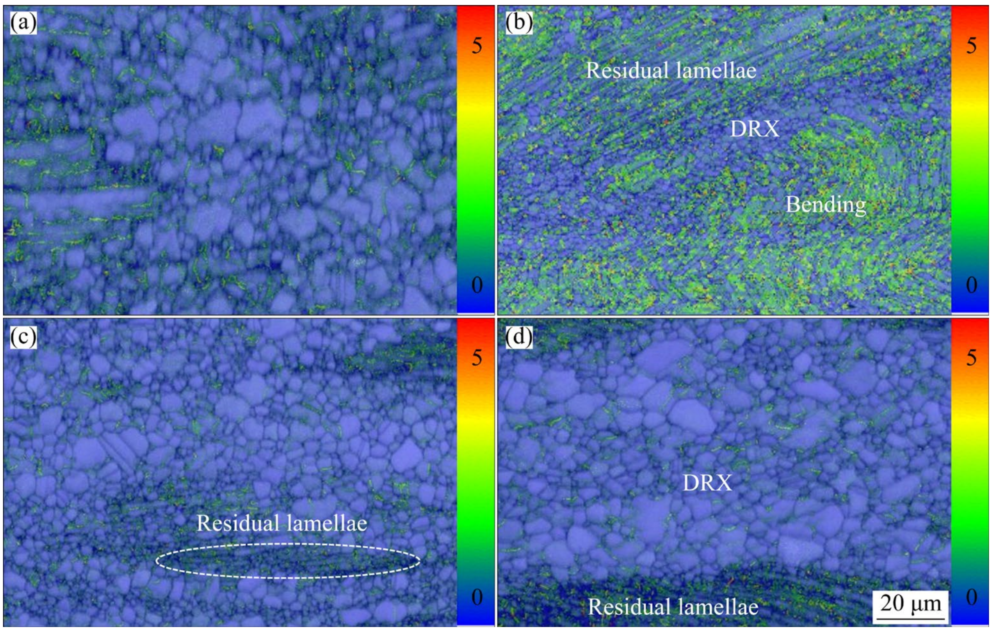

Fig. 8 Local misorientation maps with band contrast of TiAl alloy and Ti_2AlC/TiAl composite deformed at 0.01 s^{-1} and different temperatures: (a) TiAl alloy at 1200 °C; (b−d) Ti_2AlC/TiAl composite at 1100, 1150, and 1200 °C, respectively

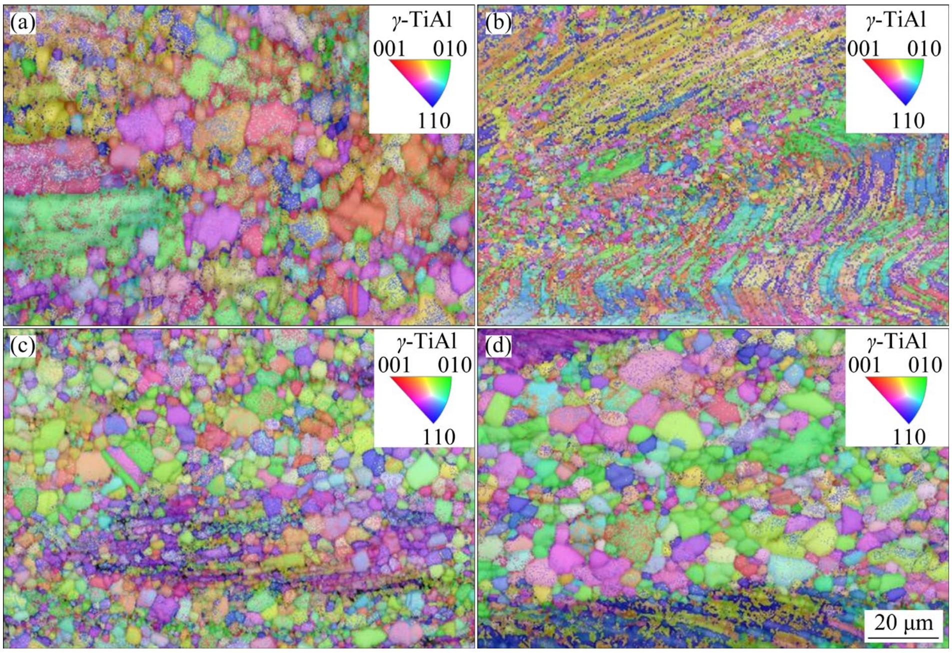

Fig. 9 IPF maps with band contrast of TiAl alloy and Ti_2AlC/TiAl composite deformed at 0.01 s^{-1} and different temperatures: (a) TiAl alloy at 1200 °C; (b−d) Ti_2AlC/TiAl composite at 1100, 1150, and 1200 °C, respectively

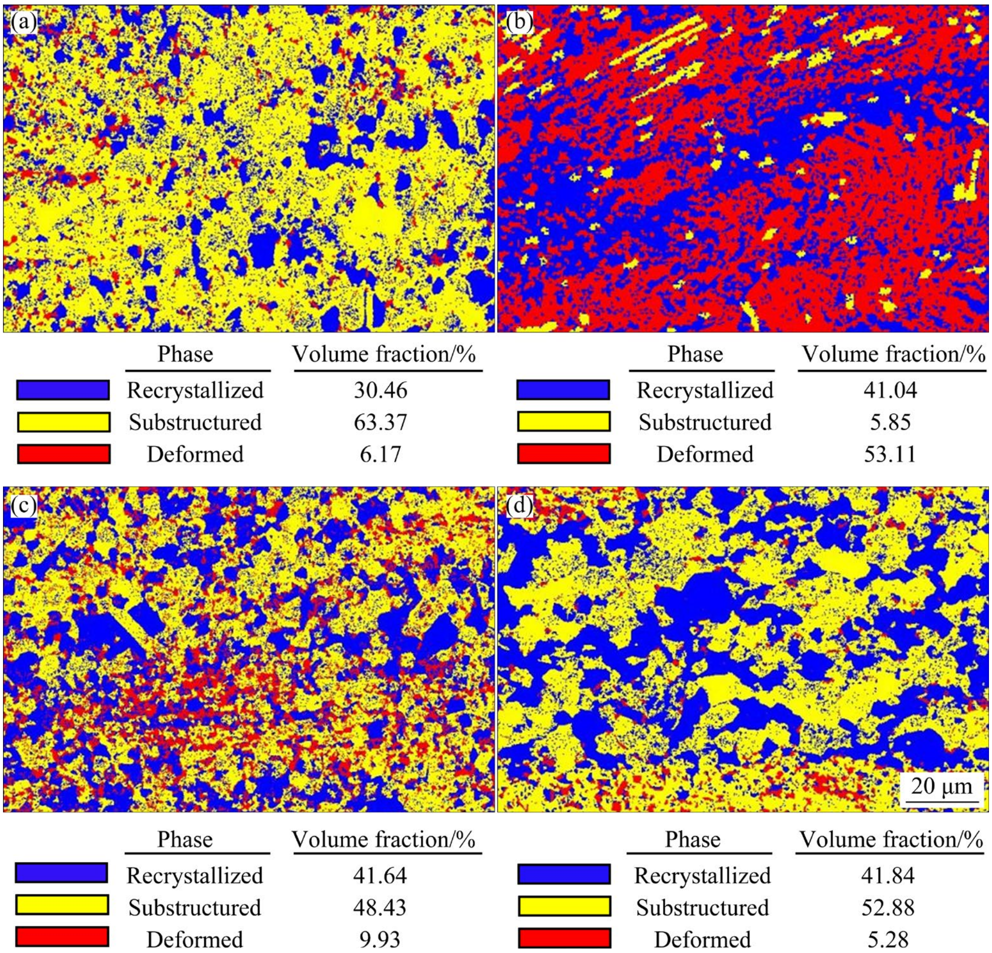

Fig. 10 Grains distribution maps and corresponding volume fractions of TiAl alloy and Ti_2AlC/TiAl composite deformed at 0.01 s^{-1} and different temperatures: (a) TiAl alloy at 1200 °C; (b−d) Ti_2AlC/TiAl composite at 1100, 1150, and 1200 °C, respectively

and equiaxed DRX grains in TiAl alloy can be observed following deformation at 1200 °C and 0.01 s^{-1}, as shown in Fig. 8(a). In addition, it was evident that the DRX region displayed low misorientation, while the residual lamellae region was characterized by high misorientation. This observation indicated that lamellar colonies were significantly deformed during hot deformation, leading to the accumulation of dislocations and residual stress [22]. However, it is noteworthy that the dislocations can be consumed by the nucleation and growth of DRX grains, resulting in the predominant distribution of low misorientation within the DRX region. Figures 8(b−d) illustrated the local misorientation maps of Ti_2AlC/TiAl composite deformed at 1100, 1150, and 1200 °C and 0.01 s^{-1}, respectively. These results revealed that the residual lamellae were characterized by high misorientation deformed at 1100 °C and 0.01 s^{-1}, as shown in Fig. 8(b). While the residual lamellae were consumed by DRX with increasing the deformation temperature, leading to the predominance of low misorientation, as shown in Figs. 8(c, d). Besides, the Ti_2AlC/TiAl composite exhibited more sufficient DRX compared to TiAl alloy under the same deformation condition, as displayed in Figs. 8(a, d). This enhancement can primarily be attributed to the refined microstructure and more DRX nucleation sites provided by the Ti_2AlC particles.

Figure 9 presented inverse pole figures (IPF). Obviously, the DRX grain size in Ti_2AlC/TiAl composite was 3.84 μm, which was smaller than that of TiAl alloy (5.48 μm) deformed at 1200 °C and 0.01 s^{-1}, as shown in Figs. 9(a, d). This was attributed to the refined lamellar colonies and Ti_2AlC particles, which provided more nucleation sites for DRX in Ti_2AlC/TiAl composite. Moreover, the grain orientation spread of the residual lamellae remained single at low deformation temperature, and most lamellae exhibited uniform orientation (Fig. 9(b)). However, the grains orientation spread became more diverse with increasing deformation temperature. This was because the residual lamellae were consumed by the nucleation and growth of non-oriented DRX grains [23].

Figure 10 exhibited the grains distribution maps, and the corresponding volume fractions of various phases in TiAl alloy and Ti_2AlC/TiAl composite were attached. The recrystallized (blue), substructured (yellow) and deformed (red) phases were observed within the deformed microstructure. The DRX was insufficient and the volume fraction of substructured phases was 63.37% in TiAl alloy deformed at 1200 °C and 0.01 s^{-1}, as shown in Fig. 10(a). However, the presence of Ti_2AlC particles refined the lamellar colonies, inhabited dislocation motion, resulted in dislocation pile-up, and promoted the formation of nano-twinning. These provided more nucleation sites for DRX. Consequently, the Ti_2AlC/TiAl composite exhibited more sufficient DRX compared to TiAl alloy in the same deformation condition, as shown in Figs. 10(a, d). Thus, it can be concluded that the Ti_2AlC particles were beneficial to DRX. As illustrated in Figs. 10(b−d), the volume fraction of recrystallized phases increased while deformed phases decreased with increasing deformation temperature for the Ti_2AlC/TiAl composite. Specifically, the volume fraction of deformed phases decreased from 53.11% to 5.28% when the deformation temperature increased from 1100 to 1200 °C.

TEM images of the Ti_2AlC/TiAl composite deformed at 1150 °C and 0.01 s^{-1} were displayed in Fig. 11. Notably, deformation twins were observed around the Ti_2AlC particles within the γ lamellae (Fig. 11(a)). The formation of twin was attributed to the stress concentration induced by the Ti_2AlC particles during deformation. Figure 11(b) exhibited a typical γ-DRX grain. It can be found that dislocations and deformation twins were observed within the interior of the DRX grain, suggesting that the DRX grain underwent the secondary deformation. It was also observed that dislocation glide and twinning were the main deformation mode. The BF micrographs of precipitates, DRX grains, and the corresponding EDS mappings were shown in Figs. 11(c−g). These results revealed the formation of DRX grains and Cr-enriched nanoparticles around Ti_2AlC particles. The Cr-enriched nanoprecipitates have been identified as hexagonal $TiCr_2$ Laves phase in our previous work [14]. The primary precipitation mechanism was the stress-induced $TiCr_2$ phase precipitation. The formation of $TiCr_2$ nanoprecipitates further strengthened the Ti_2AlC/TiAl composite through precipitation strengthening. Besides, the $TiCr_2$ nanoprecipitates hindered the dislocation motion, further inducing the dislocation pile-up during the

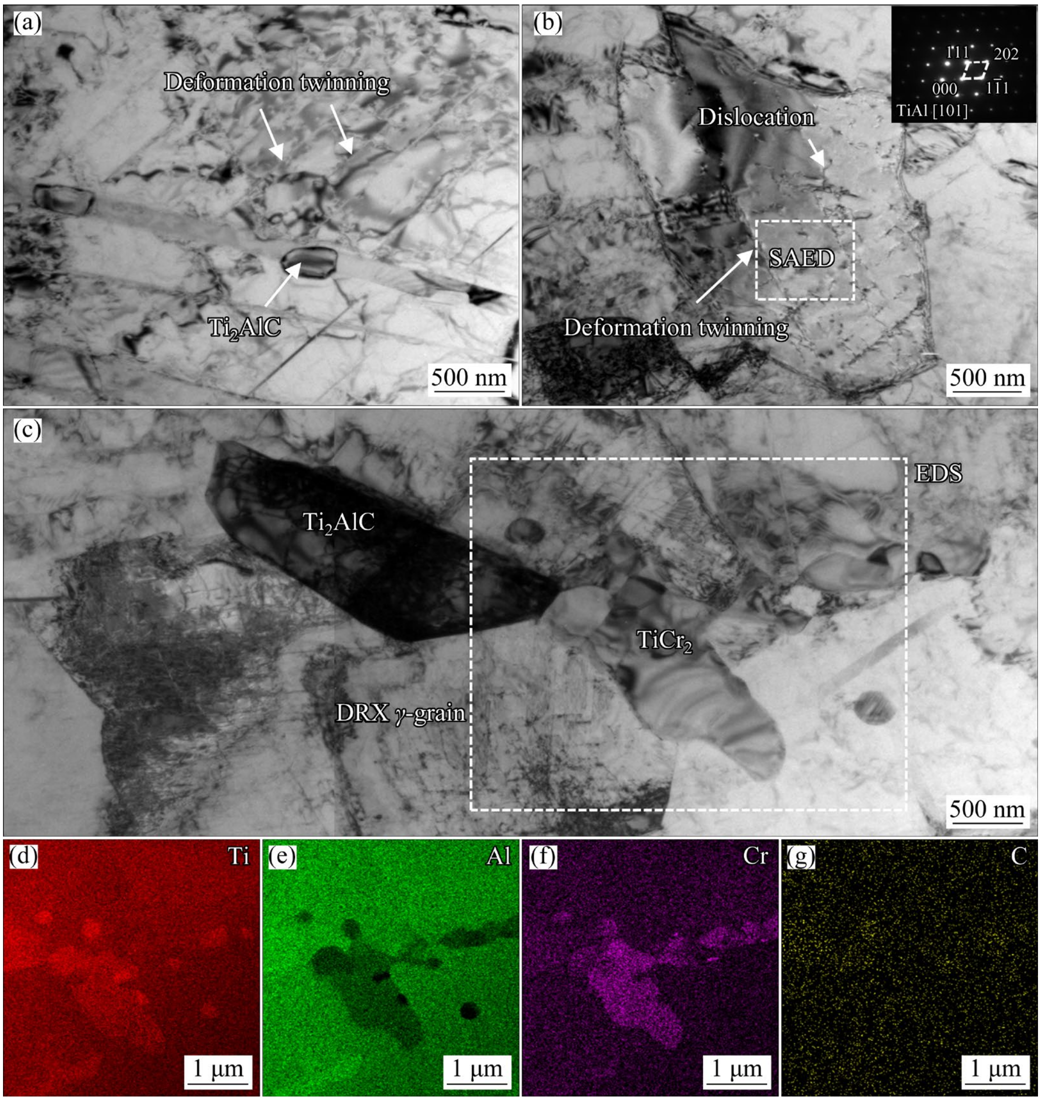

Fig. 11 TEM images of Ti_2AlC/TiAl composite deformed at 1150 °C and 0.01 s^{-1}: (a, b) BF micrographs of lamellae and DRX grain, respectively; (c−g) BF micrographs of precipitates, DRX grains and corresponding EDS mappings

deformation. These effects also contributed to the nucleation of the DRX. Besides, the deformed microstructure can be further refined by $TiCr_2$ nanoprecipitates [14,24].

Consequently, the hot workability of Ti_2AlC/TiAl composite was further improved, owing to the co-effects of refined microstructure and the precipitation of Ti_2AlC and $TiCr_2$ particles. It was notable that the micro-nano Ti_2AlC particles did not suffer obvious deformation (bending and fragmentation) during hot deformation. In the present study, the Ti_2AlC particles were micro-nano in size and homogeneously precipitated at the interfaces of lamellae, showing an excellent ability to coordinate the deformation of matrix.

The hot deformation behavior and the microstructure evolution of Ti_2AlC particles reinforced TiAl composites were also studied by YE et al [25] and LAPIN et al [26]. Their findings demonstrated that achieving a uniformly deformed structure was hard due to the uneven distribution of Ti_2AlC particles at grain boundaries. Consequently, DRX grains mainly occurred in particles-rich area. However, the current TiAl composite showed excellent hot workability, primarily attributed to the uniform distribution of micro-nano Ti_2AlC particles. This homogeneous distribution actively facilitated plastic deformation and promoted DRX. Normally, the plastic deformation was associated with the deformation twinning and dislocation slip. The deformed microstructure clearly revealed that micro-nano Ti_2AlC particles were distributed at the interfaces of γ and α_2 lamellae, thereby promoting the formation of deformation twins (Fig. 11(a)). Meanwhile, the deformation twins and dislocations were also observed within DRX γ-grains, as shown in Fig. 11(b). Deformation twinning can serve as an alternative deformation mechanism during deformation, particularly the dislocation slip is impeded due to plastic anisotropies and lo0w stacking fault energy (SFE). The mechanisms of dislocation slip also influenced the formation of deformation twins in γ-TiAl through basal-plane slip [27]. After deformation, the lamellae were decomposed, resulting in a deformed microstructure composed of DRX grains, Ti_2AlC and $TiCr_2$ particles as shown in Fig. 11(c). Notably, the DRX grains tended to appear in the particles-rich area. On the one hand, Ti_2AlC and $TiCr_2$ particles facilitated the nucleation of DRX grains. On the other hand, the numerous particles effectively hindered dislocation motion, leading to dislocation pile-up. These facilitated the formation of sub-grain boundaries or DRX grains. The present results showed that there were more γ nucleation sites in micro-nano Ti_2AlC particles reinforced TiAl composites compared to the TiAl composites reinforced with coarser Ti_2AlC particles.

Figure 12 exhibited the schematic diagrams illustrating the hot deformation mechanism for TiAl alloy and Ti_2AlC/TiAl composite. Normally, graphene oxide was distributed on the surface of TiAl powders following ball milling. Subsequently, the large primary Ti_2AlC particles formed at the boundaries between different powder particles during the sintering. The formation of primary Ti_2AlC particles was mainly attributed to the low solid solubility of carbon in the γ phase. However, residual carbon was solubilized into the matrix during the heat holding stage, owing to the higher solid solubility of carbon in the α phase compared to γ phase [28]. After sintering, the microstructure evolution was a diffusion-controlled solid-state phase transformation by $\alpha \rightarrow \alpha + \gamma \rightarrow$ lamellar α_2/γ, and simultaneously the secondary Ti_2AlC precipitated at the interfaces between the α_2 and γ lamellae.

The effect of Ti_2AlC particles on TiAl alloy included strengthening effect and softening effect. The strengthening effect can be attributed to two key factors: refined microstructure and particles strengthening. Firstly, carbon can not only affect the solidification path of TiAl alloys and refine the microstructure, but also effectively improve the strength [29,30]. Secondly, in-situ precipitated Ti_2AlC particles strengthened TiAl matrix by hindering the dislocation motion and lamellar deformation during hot deformation, consequently resulting in higher flow stress. Moreover, the harder Ti_2AlC particles distributed at the interfaces between γ and α_2 lamellae enabled the Ti_2AlC/TiAl composite to bear more loads. Ti_2AlC is a layered hexagonal phase, consisting of Ti_2C and Al layer (stacked on top of each other along the [0001]

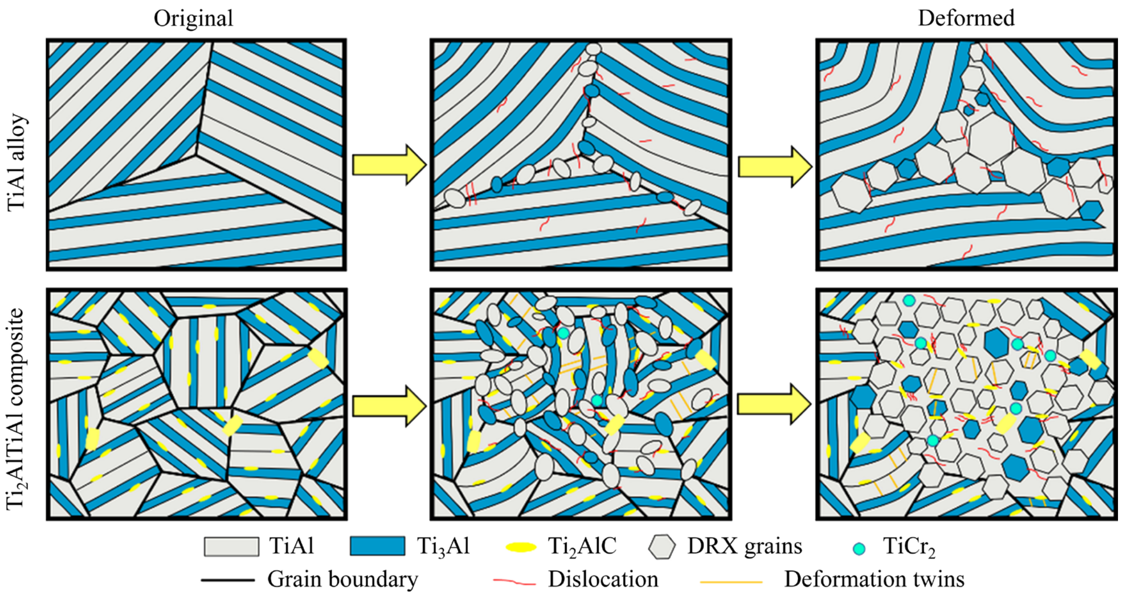

Fig. 12 Schematic diagrams of deformation mechanisms of TiAl alloy and Ti_2AlC/TiAl composite

direction), which results in anisotropic plastic deformation behavior [31]. As a result, Ti_2AlC can coordinate the deformation through a multitude of deformation modes (including basal-plane dislocation, atomic-scale ripples and kink bands) [32]. The multiple deformation modes played a crucial role in improving the damage tolerance and fracture toughness of MAX phases, which can coordinate the deformation of Ti_2AlC/TiAl composite by absorbing loading energy, reducing the stress concentration, and hindering the crack propagation. Thirdly, Ti_2AlC particles promoted the precipitation of $TiCr_2$ nanoparticles, which further strengthened the Ti_2AlC/TiAl composite by precipitation strengthening.

The softening effect was mainly attributed to Ti_2AlC-induced DRX softening. The presence of Ti_2AlC particles effectively refined the lamellar colonies, thereby providing more nucleation sites for DRX during hot deformation. In addition, the precipitation of micro-nano Ti_2AlC particles induced local stress concentration resulted in the formation of nano-twinning. This twin formation inhabited dislocation motion, leading to dislocation pile-up and promoting more DRX nucleation. As a result, more sufficient DRX and uniform deformation microstructure can be obtained in Ti_2AlC/TiAl composite. Therefore, the Ti_2AlC/TiAl composite showed superior hot workability compared to TiAl alloy.

4 Conclusions

(1) The Ti_2AlC/TiAl composite with fully lamellar microstructure was in-situ synthesized by SPS using Ti−48Al−2Nb−2Cr powder and graphene oxide. The micro-nano Ti_2AlC particles were uniformly precipitated at the interfaces between α_2 and γ lamellae.

(2) The Ti_2AlC/TiAl composite demonstrated a higher flow stress, which was attributed to the fine-grain strengthening and particles strengthening induced by Ti_2AlC particles. In addition, the formation of nano-twinning and $TiCr_2$ nanoprecipitates hindered dislocation slip and led to strengthening effect.

(3) Ti_2AlC/TiAl composite showed superior hot workability compared to TiAl alloy. This enhancement can be attributed to the Ti_2AlC particles, promoting DRX by grain refinement, nano-twinning formation and nano-$TiCr_2$ precipitation.

CRediT authorship contribution statement

Yu-peng WANG: Methodology, Writing − Original draft, Validation; **Teng-fei MA:** Validation, Writing − Original draft; **Lei LI:** Writing − Review & editing, Validation; **Long-long DONG:** Software, Data collection; **Wang-tu HUO:** Conceptualization, Writing − Review & editing; **Yu-sheng ZHANG**: Writing − Review & editing; **Lian ZHOU**: Conceptualization, Writing − Review & editing, Validation.

Declaration of competing interest

The authors declare that they have no known competing financial interests or personal relationships that could have appeared to influence the work reported in this paper.

Acknowledgments

This work was supported by the National Natural Science Foundation of China (No. 52001262), the Natural Science Foundation of Zhejiang Province, China (No. LZY22E010001), and the Natural Science Foundation of Shaanxi Province, China (No. 2020JC-50)

References

[1] DING Jie, ZHANG Ming-he, LIANG Yong-feng, REN Yang, DONG Cheng-li, LIN Jun-pin. Enhanced high-temperature tensile property by gradient twin structure of duplex high-Nb-containing TiAl alloy [J]. Acta Materialia, 2018, 161: 1−11.

[2] LIU Pei, HOU Bo, WANG Ai-qin, XIE Jing-pei, WANG Zhen-bo. Balancing the strength and ductility of Ti_2AlC/TiAl composite with a bioinspired micro-nano laminated architecture [J]. Materials & Design, 2022, 220: 110851.

[3] LUO Yao-feng, LU Rui-yu, WANG Yan, LIU Bin, YANG Hai-tang, LIU Yong. Interfacial reaction in Al_2O_3 fiber reinforced TiAl matrix composite [J]. Transactions of Nonferrous Metals Society of China, 2023, 33: 2054−2063.

[4] SONG Xiao-jie, CUI Hong-zhi, HAN Ye, HOU Nan, WEI Na, DING Lei, SONG Qiang. Effect of carbon reactant on microstructures and mechanical properties of TiAl/Ti_2AlC composites [J]. Materials Science and Engineering A, 2017, 684: 406−412.

[5] LI Ming-ao, LI Juan, ZHOU Tao, HU Li, SHI Lai-xin, CHEN Yu-yong, XU Li-juan, XIAO Shu-long. Microstructure evolution, deformation behavior and manufacture design of TiAl matrix composites reinforced with in-situ borides precipitation [J]. Transactions of Nonferrous Metals Society of China, 2023, 33: 107−127.

[6] DING Hao, CUI Xi-ping, GAO Nao-nao, SUN Yuan, ZHANG Yuan-yuan, HUANG Lu-jun, GENG Lin.

Fabrication of (TiB/Ti)−TiAl composites with a controlled laminated architecture and enhanced mechanical properties [J]. Journal of Materials Science & Technology, 2021, 62: 221−233.

[7] FANG Hong-ze, WANG Shu, CHEN Rui-run, XU Qian, YAN Yong-da, SU Yan-qing, GUO Jing-jie. The effects of the formation of a multi-scale reinforcing phase on the microstructure evolution and mechanical properties of a Ti_2AlC/TiAl alloy [J]. Nanoscale, 2021, 13: 12565−12576.

[8] REN Li-rong, QIN Shui-jie, ZHAO Si-hao, XIAO Hua-qiang. Fabrication and mechanical properties of Ti_2AlC/TiAl composites with co-continuous network structure [J]. Transactions of Nonferrous Metals Society of China, 2021, 31: 2005−2012.

[9] CHENG Jun, ZHU Sheng-yu, YU Yuan, YANG Jun, LIU Wei-min. Microstructure, mechanical and tribological properties of TiAl-based composites reinforced with high volume fraction of nearly network Ti_2AlC particulates [J]. Journal of Materials Science & Technology, 2018, 34: 670−678.

[10] WU Ming-yu, MI Guang-bao, LI Pei-jie, HUNAG Xu. Formation mechanisms of Ti_2AlC and Ti_3AlC during solid-state sintering between multilayer graphene and TiAl alloy composite [J]. Acta Physica Sinica, 2022, 71: 196801.

[11] WU Ming-yu, MI Guang-bao, LI Pei-jie, HUANG Xu, GAO Chun-xiao. Study on interface reaction between multilayer graphene and TiAl alloy [J]. Materials Letters, 2022, 310: 131515.

[12] GUO Ying-chao, LIANG Yong-feng, LIN Jun-pin. In situ synthesis of nano/micron Ti_2AlC reinforced high-Nb TiAl composites: Microstructure and mechanical properties [J]. Intermetallics, 2023, 159: 107937.

[13] MA Teng-fei, LI Qiao-yu, WANG Yu-peng, WANG Xiao-hong, DONG Duo, ZHU Dong-dong. Microstructure and mechanical properties of micro-nano Ti_2AlC-reinforced TiAl composites [J]. Intermetallics, 2022, 146: 107563.

[14] LIU Cheng-ze, WANG Yu-peng, HAN Wei-zhong, MA Teng-fei, MA Dong-feng, ZHANG Yu-sheng. Achieving superior high-temperature strength and oxidation resistance of TiAl nanocomposite through in situ semi-coherent MAX phase precipitation [J]. ACS Applied Materials & Interfaces, 2022, 14: 8394−8403.

[15] WANG Yu-peng, LIU Cheng-ze, MA Teng-fei, LIU Yue, ZHANG Yu-sheng, ZHOU Lian. Improvement in oxidation resistance of TiAl alloys by in-situ precipitation of Ti_2AlC at the interface of α_2 and γ lamellae [J]. Corrosion Science, 2022, 208: 110639.

[16] TIAN Shi-wei, HE An-rui, LIU Jian-hua, ZHANG Ye-fei, ZHANG Si-yuan, ZHANG Yun, YANG Yong-gang, JIANG Hai-tao. Investigation on the microstructure evolution and dynamic recrystallization mechanisms of TiAl alloy at elevated temperature [J]. Journal of Materials Research and Technology, 2021, 14: 968−984.

[17] SONG Lin, APPEL F, WANG Li, OEHRING M, HU Xing-guo, STARK A, HE Jun-yang, LORENZ U, ZHANG Tie-bang, LIN Jun-pin, PYCZAK F. New insights into high-temperature deformation and phase transformation mechanisms of lamellar structures in high Nb-containing TiAl alloys [J]. Acta Materialia, 2020, 186: 575−586.

[18] WANG Bo, HUANG Lu-jun, LIU Bao-xin, GENG Lin, HU Hai-tao. Effects of deformation conditions on the microstructure and substructure evolution of TiBw/Ti60 composite with network structure [J]. Materials Science and Engineering A, 2015, 627: 316−325.

[19] XU Zeng-shi, SHI Xiao-liang, ZHAI Wen-zheng, YAO Jie, SONG Si-yuan, ZHANG Qiao-xin. Preparation and tribological properties of TiAl matrix composites reinforced by multilayer graphene [J]. Carbon, 2014, 67: 168−177.

[20] LU Ke, LU Lei, SURESH S. Strengthening Materials by engineering coherent internal boundaries at the nanoscale [J]. Science, 2009, 324: 349−352.

[21] CHEN Rui-run, MA Teng-fei, GUO Jing-jie, DING Hong-sheng, SU Yan-qing, FU Heng-zhi. Deformation behavior and microstructural evolution of hydrogenated Ti44Al6Nb alloy during thermo-compression at 1373−1523 K [J]. Materials & Design, 2016, 108: 259−268.

[22] WANG Qi-bin, ZHANG Shu-zhi, YANG Jie-ren, DONG Duo, ZHU Dong-dong. The influence of the dynamic softening mechanism of α phase and γ phase on remnant lamellae during hot deformation [J]. Journal of Alloys and Compounds, 2021, 872: 159514.

[23] DONG Shu-lin, DING Xin, CHEN Rui-run, GUO Jing-jie, FU Heng-zhi. High-temperature deformation resistance and creep resistance of a TiAl-based alloy fabricated by cold crucible directional solidification technology [J]. China Foundry, 2020, 17(5): 378−383.

[24] LIU Cheng-ze, LI Ge-ping, YUAN Fu-sen, HAN Fu-zhou, ZHANG Ying-dong, GU Heng-fei. Stacking faults in $Zr(Fe,Cr)_2$ Laves structured secondary phase particle in Zircaloy-4 alloy [J]. Nanoscale, 2018, 10: 2249−2254.

[25] YE Pei-hao, JIN Xu-chen, FANG Wen-bin, LI Xue-wen, WU Hao, FAN Guo-hua. Hot deformation behavior and microstructure evolution of a high Nb containing PM TiAl composite reinforced with Ti_2AlC particles [J]. Materials Today Communications, 2021, 29: 102862.

[26] LAPIN J, ŠTAMBORSKÁ M, PELACHOVÁ T, ČEGAN T, VOLODARSKAJA A. Hot deformation behaviour and microstructure evolution of TiAl-based alloy reinforced with carbide particles [J]. Intermetallics, 2020, 127: 106962.

[27] WANG Zhen-bo, LIU Pei, WANG Ai-qin, XIE Jing-pei, HOU Bo. Fabrication, microstructure and mechanical properties of TiAl matrix composite reinforced by submicro/nano-Ti_2AlC [J]. Materials Characterization, 2023, 203: 113141.

[28] KLEIN T, SCHACHERMAYER M, MENDEZ-MARTIN F, SCHOBERL T, RASHKOVA B, CLEMENS H, MAYER S. Carbon distribution in multi-phase γ-TiAl based alloys and its influence on mechanical properties and phase formation [J]. Acta Materialia, 2015, 94: 205−213.

[29] WU Ze-en, HU Rui, ZHANG Tie-bang, ZHANG Fan, KOU Hong-chao, LI Jin-shan. Understanding the role of carbon atoms on microstructure and phase transformation of high Nb containing TiAl alloys [J]. Materials Characterization, 2017, 124: 1−7.

[30] KIM Y W, KIM S L. Effects of microstructure and C and Si additions on elevated temperature creep and fatigue of gamma TiAl alloys [J]. Intermetallics, 2014, 53: 92−101.

[31] LIU Pei, HOU Bo, WANG Ai-qin, XIE Jing-pei, WANG

Zhen-bo, YE Feng. Superior strength−plasticity synergy in a heterogeneous lamellar Ti_2AlC/TiAl composite with unique interfacial microstructure [J]. Journal of Materials Science & Technology, 2023, 159: 21−32.

[32] ZHAN Zhi-qiang, CHEN Ye-xiao, RADOVIC M, SRIVASTAVA A. Non-classical crystallographic slip in a ternary carbide−Ti_2AlC [J]. Materials Research Letters, 2020, 8(7): 275−281.

原位合成 Ti_2AlC/TiAl 复合材料的显微组织演变及热加工性能

王玉鹏[1]，马腾飞[1,2]，李 磊[1]，董龙龙[1]，霍望图[1]，张于胜[1]，周 廉[1]

1. 西北有色金属研究院，西安 710016；
2. 衢州学院 浙江省空气动力装备技术重点实验室，衢州 324000

摘 要：利用放电等离子烧结技术原位合成微纳米 Ti_2AlC 颗粒增强的 TiAl 复合材料(Ti_2AlC/TiAl)。研究了 Ti_2AlC/TiAl 复合材料的热加工性能，讨论了微纳米颗粒对复合材料流变应力和动态再结晶的影响。结果表明，微纳米 Ti_2AlC 颗粒在热变形过程中同时具有强化效应和软化效应，最终导致 Ti_2AlC/TiAl 复合材料呈现出更高的流变应力和更充分的动态再结晶。变形初期，微纳米 Ti_2AlC 颗粒细化组织和阻碍位错滑移引起强化效应。此外，变形过程中应力集中诱导了纳米 $TiCr_2$ 相的析出，进一步阻碍位错滑移导致更高的流变应力。另一方面，组织的细化和微纳颗粒在变形过程中引起的位错塞积为动态再结晶提供了更多的形核位点，显著促进了变形第二阶段的动态再结晶。研究表明，Ti_2AlC/TiAl 复合材料具有优异热加工性能，对促进 TiAl 合金应用具有重要意义。

关键词：Ti_2AlC/TiAl 复合材料；放电等离子烧结；热变形；组织演变；动态再结晶

(Edited by Wei-ping CHEN)